IEEE Access
Multidisciplinary | Rapid Review | Open Access Journal

Received 10 March 2023, accepted 2 April 2023, date of publication 7 April 2023, date of current version 13 April 2023.

Digital Object Identifier 10.1109/ACCESS.2023.3265580

RESEARCH ARTICLE

Posture Estimation by Clustering Pressure Information and Control Implementation for Pneumatically Driven Gait-Assistive Robot

TETTA KADOKURA[1], TETSURO MIYAZAKI[1], (Member, IEEE), TOSHIHIRO KAWASE[2], (Member, IEEE), MAINA SOGABE[1], AND KENJI KAWASHIMA[1], (Member, IEEE)

[1]Department of Information Physics and Computing, The University of Tokyo, Bunkyo-ku, Tokyo 113-8656, Japan
[2]Department of Information and Communication Engineering, Tokyo Denki University, Adachi-ku, Tokyo 120-0026, Japan

Corresponding author: Tetsuro Miyazaki (Tetsuro_Miyazaki@ipc.i.u-tokyo.ac.jp)

This work was supported in part by Bridgestone Corporation and KAKENHI under Grant 20K19594 and Grant 21H04544, and in part by the Cooperative Research Project of the Research Center for Biomedical Engineering.

This work involved human subjects or animals in its research. Approval of all ethical and experimental procedures and protocols was granted by the Ethics Committee of the Graduate School of Information Science and Technology, the University of Tokyo under Review No. UT-IST-RE-210702-1.

ABSTRACT Pneumatic artificial muscles (PAMs) are light and soft, and are expected to be applied to gait assistance robots with multiple actuators on the human body. The PAMs can be used as not only actuators, but also sensors to detect the gait phase by using their deformable bodies whose internal pressure changes in response to the wearer's gait. However, conventional methods to detect the gait phase by PAMs have targeted single point detection in a gait phase and used for only ON/OFF control of the PAM actuators. In this study, we proposed an algorithm to estimate the postural state of the wearer, especially the state of both hip joints, from the internal pressure information of the PAMs with a small amount of calculation by using clustering method, and succeeded in controlling the PAMs' pressure continuously based on this algorithm. The effectiveness of the proposed control method was verified through gait-assistive experiments using a treadmill. We measured the electromyogram of the adductor longus muscle under 3 subjects and a one-sided significant difference test was performed. As a result, we confirmed significant differences at the 1% significance level for 2 subjects and at the 10% significance level for the remaining subject, allowing us to evaluate the effectiveness of the proposed PAM control strategy.

INDEX TERMS Posture estimation algorithm, gait-assistive robot, pneumatic artificial muscle, back-drivability, soft robot.

I. INTRODUCTION

A. BACKGROUND

In recent years, power-assistive devices have been developed for various applications [1], [2], [3], ranging from the fields of nursing care [4], [5], gait assistance [6], [7], [8], [9], [10], [11], [12], [13], [14], [15], rehabilitation [16], [17], [18], [19], [20] and other welfare applications, to industrial [21], [22], [23] and military [24] applications. For example, Sankai [4] developed a robot suit HAL (Hybrid Assistive Limb) driven by electric motors, which detects the wearer's intention to walk by bioelectric sensors directly attached to the user, in addition to angle sensors and other sensors built into the robot. Li et al. [8] designed a prototype of a lightweight, low-power-consumption walking assistive wear with soft actuators using plasticized polyvinyl chloride (PVC) gel and mesh electrodes. Asbeck et al. [13], [14], [15] developed a soft exo-suit which is light weight system driven by Bowden cables, and BLEEX (Berkeley Lower Extremity Exoskeleton) [24] was developed to improve carrying capacity and is driven

The associate editor coordinating the review of this manuscript and approving it for publication was Tao Wang.

by hydraulic actuators. Different mechanisms and control methods are applied to each of these devices, and appropriate sensors and actuators are utilized depending on the situation. One of the technical challenges in realizing assistive devices is to synchronize the assist force with the wearer's movement. Traditionally, to detect the wearer's motion state, most devices use electrical sensors, such as bioelectrical sensors [4], [5], joint angle sensors [4], [11], [19], inertial measurement units (IMU) [13], [14], [15], force/torque sensors [12], [16], and undersole pressure sensors [4], [8], [10], [13], [14], [15], [24]. It was necessary to wear them on the user's body surface or to build them into the assistive device. By fusing multimodal information obtained from different types of sensors, the reliability of detecting the user's exercise state can be improved. However, it increases the time required to start the device for the calibration process and reduces the usability of the device. Therefore, from the viewpoint of ease of installation, it is desirable to reduce the number of sensors to be attached to the assistive device.

On the other hand, many power-assistive robots using Pneumatic Artificial Muscle (PAM), have been developed in recent years [25]. Kadota et al. [26] proposed a power-assistive robotic arm that mimics the motion of bi-articular muscles using PAM covered with an exoskeleton suit. Tadano et al. [27] developed a grip force amplification glove using PAMs and succeeded in realizing a bi-articular mechanism suitable for finger flexion and extension, and Sridar et al. [28] developed a soft inflatable exosuit to assist knee extension during gait training in stroke rehabilitation. This device uses an IMU and shoe insole sensors. Kanno et al. [6] proposed a pneumatically driven gait-assistive device and its control method that utilizes the back-drivability of PAM. In this control method, the gait phase of the wearer is detected by using air pressure sensors isolated from the device itself, without attaching electric sensors to the wearer's body.

Several methods have been developed for detecting the state of the walker. For example, Lim et al. [29] determined various dynamic models of the lower extremity exoskeleton from ground reaction force (GRF) data obtained from insole sensors. Ding et al. [30] proposed a method to detect and identify gait phase from data obtained from a single inertial measurement unit (IMU) by using an algorithm based on long-term short-term memory (LSTM). Wang et al. [31] proposed a gait state recognition system based on a support vector machine using plantar pressure sensors and acceleration sensors on the human legs. Lee et al. [32] proposed a deep learning-based gait type classification method using smart insoles equipped with various sensor arrays. Other studies by Villarreal [33] and Quintero [34] proposed a gait phase variable by using a declination angle defined by measured thigh angle and thigh angular velocity during walking. However, both of the above methods require at least one or more electrical sensors to be attached to the body surface.

In contrast, the study by Kanno et al. [6] used only PAM for gait phase detection and did not require to attach any electrical sensors to the wearer's body. PAM has a property called back-drivability, which means that deformation of the PAM due to walking is transmitted to the control input side through the pneumatic circuit as internal pressure information. By utilizing this property, it is possible to detect the stage of gait from the internal pressure information of the artificial muscle. In that study, a point on the pre-swing phase of the gait cycle was detected at each cycle based on a threshold-based judgment condition for the internal pressure value. Then, after calculating the gait cycle based on the temporal distance between these points, the PAMs were controlled to contract or not based on the time period in the gait cycle. Furthermore, in a study by Miyazaki et al. [7], a threshold decision condition was added to the above method, enabling the suit to be controlled successfully even when the walking speed changes. With the above mechanisms, these devices [6], [7] did not require a single electrical sensor to be attached to the body surface, allowing easy attachment and removal of the gait-assistive robot. However, the following issues remain to be solved.

- The internal pressure information detects only one point in the pre-swing phase, and the other time periods are interpolated by assuming an average gait. The conventional method can assist the average gait effectively; however, there is no guarantee that the gait state of the wearer is typical. In the case of a gait far from average, assist timing will become inappropriate, and the assist force will prevent safe walking. The internal pressure of the PAM changes throughout the gait cycle, and the conventional detection algorithm does not make the best use of the measured pressure information.
- The simple ON/OFF control was performed based on the assumption of a typical human gait as defined by Perry et al. [35]. Since human gait is a continuous movement, more personalized assistance can be provided by continuously controlling the artificial muscles in accordance with the user's movement state. Moreover, in the ON/OFF control, the internal pressure shows periodic sharp rises and falls, and the tension changes abruptly, which may cause danger and difficulty in walking.

In addition, there are some previous studies [36], [37] that used the concept of reservoir computing to estimate the posture of the wearer from the internal pressure information of the PAM. In those studies, multiple PAMs connected by a pneumatic circuit were considered as physical reservoirs, and the thigh angle was estimated by Ridge regression of multiple nonlinear pressure signals measured along the circuit. However, the above method required the measurement of internal pressure at multiple locations on the pneumatic circuit. For practical use, it is desirable to be able to estimate the posture state from the internal pressure information of a single PAM. However, since this method is based on adding up internal

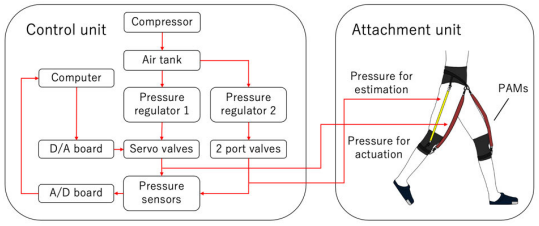

FIGURE 1. Overall pneumatic system (yellow: PAM for estimation; red: PAM for actuation).

TABLE 1. The parameters of the robot and the PAM.

Parameter	Value
Whole mechanism weight [kg]	1.2
The number of PAMs	3
PAM for estimation weight [kg]	40.5×10^{-3}
PAM for actuation weight [kg]	63.0×10^{-3}
PAM for estimation length [m]	250×10^{-3}
PAM for actuation length [m]	250×10^{-3}
PAM for estimation inner diameter [m]	5.0×10^{-3}
PAM for actuation inner diameter [m]	9.5×10^{-3}

pressure values from multiple locations, the estimation accuracy may deteriorate if the number of measurement points is reduced. In addition to angle, if more complex waveform signals such as angular velocity and angular acceleration are to be estimated, it may be necessary to apply a different estimation algorithm instead of the linear regression method.

B. CONTRIBUTIONS OF THIS STUDY

The contributions of this study are as follows. First, by assuming the broad-sense periodicity of walking motion, we proposed a new algorithm to estimate the posture state of the wearer from the internal pressure information of a single PAM with a small amount of computation. Second, we carried out continuous pressure-following control of the PAM based on the estimated joint states of the lower limb and the assumed mechanical model of the walker. Finally, we analyzed the amount of muscle activity through gait-assistive experiments on multiple subjects and confirmed the effectiveness of the proposed control strategy.

These contributions suggest the feasibility of novel personalized assistance based on state estimation throughout the entire gait cycle. Since there are no moments when the gait state cannot observe, the proposed assist has an advantage in terms of safety.

This paper is organized as follows. In Section II, we describe the overall mechanism of the proposed method and explain the posture estimation algorithm. In Section III, we introduce a control method for a gait-assistive robot based on the wearer's link model. In Section IV, we discuss the experiments conducted to confirm the effectiveness of the proposed control strategy. In the end, We draw the conclusions in Section V.

II. PROPOSED ESTIMATION METHOD

A. PNEUMATIC SYSTEM

The overall pneumatic system of the suit is shown in Fig. 1. The control unit consists of a compressor, air tank, pressure regulator, computer, servo valve, manual valve (2-port valve), pressure sensor, A/D board, D/A board, etc. The pressure in the PAM is transmitted through the air tube and measured by the pressure sensors (SMC, PSE510 and PSE532) in the control unit and sent to the computer by the A/D board. The command voltage of the servo valve (Festo, MPYE5-1/4-010-B) is calculated by the computer and sent from the D/A board. The pressure of the PAM for actuation is controlled by the controller. The gait-assistive robot also uses the back-drivability of the PAM to estimate the wearer's joint condition. To realize that, the pressure information of the PAM is used. Therefore, the PAM for estimation, which is fixed to the lateral right thigh, is pressurized in advance and the air flow is closed by a manual valve. The PAM in the lateral thigh becomes a closed chamber that can be deformed, and the pressure information resulting from the deformation is used to estimate the wearer's condition. The compressor, which is one of the main noise sources, is separated from the pneumatic system of the gait assistive robot using a long air tube. In addition, noise from the servo valves is reduced by the attached silencer; therefore, it can be used without problems in places such as training facilities.

While most conventional suits are rigid linkage systems, the attachment unit of the suit consists of the lightweight parts, such as waist supporter, knee supporter, and nylon belt. The entire attachment unit weighs approximately 1.2 kg. The attachment unit has no built-in electrical sensors. The supporter is made of soft fibers such as polyester, nylon, polyurethane, and natural rubber. The lower back supporter is secured to the pelvis by the tightness of the fibers and nylon belt. Knee supporters are similarly secured to the knee joint. These supporters are connected so that the PAM does not slip on the body surface, effectively transferring the contraction force of the PAM to the leg movements. The suit is applied for a short period of time, less than 5 minutes. The suit has the advantage of being easier and safer to use than conventional rigid-type suits because it does not require the trainee to wear an electrical sensor and the suit is soft and lightweight.

In this study, a total of three PAMs (Bridgestone), two for assist and one for estimation, are attached to the body surface. When fitting the PAMs for estimation and assist, we use adjustable bands to adjust the devices for each subject to ensure that tension is maintained. The only muscles targeted for assist are the adductor longus (AL) muscles of both legs located in the anterior part of thighs. When the PAMs of both anterior thighs are contracted by appropriate pressure, the hip flexion motion can be assisted. The parameters of the robot and the PAM are shown in Table 1.

B. PROPOSED POSTURE ESTIMATION ALGORITHM

In this section, we specifically describe our proposed method for estimating the postural state of the wearer. In short, this

method is an algorithm for estimating the wearer's joint state from the internal pressure information of a single PAM with a small amount of computation by utilizing the broad sense periodicity of gait data and a clustering method. The idea of the method is as follows.

When our gait-assistive robot is used, the user walks on a treadmill; thus, the walking speed can be fixed, and the measurement data obtained from such periodic motion are also expected to be periodic. However, human gait is not strictly repetitive because of variations in the stride length and tempo. This characteristic of the data is called periodicity in the broad sense in this paper. When sufficiently long training data can be obtained, data similar to the ''pressure data observed as input during estimation'' should be available as training data. Therefore, the data closest to the measured internal pressure information should be identified in the training data, and the joint state at that point in time should be used as the estimated value. This is similar to the ''nearest neighbor'' method in classification algorithms. However, comparing all the data is computationally very time-consuming, and is not a desirable estimation method in situations where real-time performance is required, such as robot control. Therefore, we have considered clustering the training data by gait phase to greatly reduce the number of comparisons. The steps in the learning process are as follows.

The internal pressure of the PAM for estimation and the wearer's joint state are measured simultaneously as training data. The joint state mentioned above means the angle, angular velocity, and angular acceleration at both right and left hip joints in this paper.

Next, we cluster the weighted coordinates $\left(k_p p[k], k_{\dot{p}} \dot{p}[k]\right)$, where $p[k]$ is the PAM pressure at each time k and $\dot{p}[k]$ is its derivative. Clustering is performed using the k-means method [38]. k-means is the simplest of the non-hierarchical clustering methods, which is based on the center of gravity in each cluster. When the number of clusters is N, the vector of each data is x_k, the vector of centers of gravity in each cluster n is μ_n, and the set of data belonging to each cluster is C_n, the algorithm minimizes the evaluation function J expressed by the following formula. For a more detailed explanation, see MacQueen et al. [38]

$$x_k = \begin{pmatrix} k_p p[k] \\ k_{\dot{p}} \dot{p}[k] \end{pmatrix} \tag{1}$$

$$k_p = 1/\,\mathrm{std}(p),\ k_{\dot{p}} = \alpha/\,\mathrm{std}(\dot{p}) \tag{2}$$

$$J = \sum_{n=1}^{N} \sum_{x_k \in C_n} (x_k - \mu_n)^2 \tag{3}$$

α is a parameter that indicates the balance of importance of the data and is determined through experiment. In this study, we assumed $\alpha = 1.0$. Next, we record the average pressure value p_n, its derivative $\dot{p}_n$, and the average joint state vector $\vec{S}_n$ in each cluster n on the lookup table.

During estimation, the wearer's joint state can be estimated by searching for the closest data to the observed pressure data on the lookup table and using the average joint state vector in that cluster as the estimated value. Fig. 2 shows the clustering with 10 clusters. There is an order relationship among the clusters, i.e., the cluster to which the data appearing immediately after the data belonging to a cluster belongs is mostly determined. Therefore, if the cluster which is closest to the previous data is known, there is no need to search all clusters, and comparing the two clusters should be sufficient. Therefore, in our method, we add another twist.

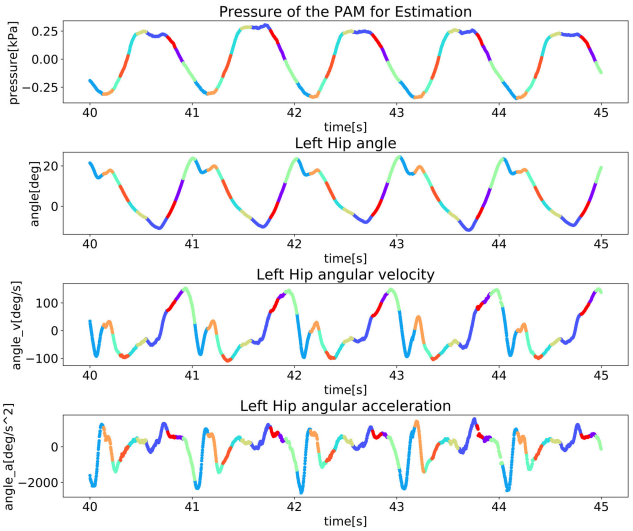

FIGURE 2. Clustering example (The number of clusters is 10).

The cluster with the highest number of transitions in each cluster is recorded in advance from the time series data. Since walking on a speed-fixed treadmill is a periodic movement, the above procedure is expected to ideally connect all the clusters in a circular manner.

As mentioned earlier, our method estimates the joint state through two comparisons. When the previous data is closest to cluster $\hat{c}_i$, the distance to $(p, \dot{p})$ is calculated only for the average pressure information in cluster $\hat{c}_i$ and that in its transition point, cluster $\hat{c}_{i\_next}$. During estimation, the cluster that is closer of the two is selected as:

$$\hat{c}_{i+1} = \mathrm{argmin}\left[\left\{k_p\,(p - p_c)\right\}^2 + \left\{k_{\dot{p}}\,(\dot{p} - \dot{p}_c)\right\}^2\right] \tag{4}$$

$$c \in C_{\mathrm{compared}} = \left\{\hat{c}_i, \hat{c}_{i\_next}\right\} \tag{5}$$

In practice, however, transitions between clusters may continue to fail, resulting in larger estimation errors. If the same cluster is continuously selected for a certain number of consecutive times, the estimation error is considered to spread, and an exception is made by temporarily switching the search to all clusters.

The flowchart of the entire algorithm is shown in Fig. 3. The various variables appearing in the flowchart are explained as follows. n is the number of times estimation remained in the same cluster consecutively. n_{th} is upper threshold for n. It was set to 50 in this study (Sample rate is 500 Hz). C_{all} is all clusters. *data* is measured PAM pressure and its derivative data. Compare is function that compares

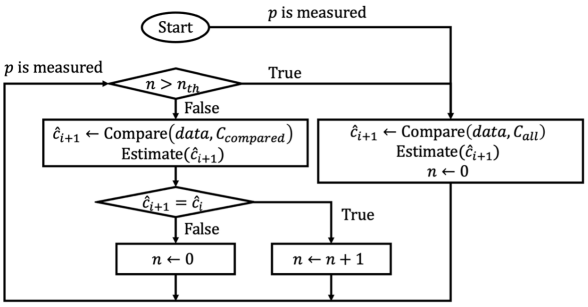

FIGURE 3. Overall estimation algorithm.

clusters. Estimate is function to obtain the posture state of the desired cluster from the lookup table.

Note that our method builds a model for each subject, but the training time is short, only a few seconds to about a minute per subject, under Ubuntu 18.04.6 Intel Core-i9 with eight physical cores.

C. OFFLINE ESTIMATION EXPERIMENT

We first conducted an offline posture state estimation experiment. One healthy adult walked on a treadmill wearing a suit, angle sensors on both hip joints, and a PAM for estimation on the side of the right thigh. The experiment is illustrated in left side of Fig. 4. The PAM for estimation was pressurized in advance by a hand valve at a constant pressure (approximately 100 kPa) and sealed to allow deformation. Walking was performed at a speed of 5 km per hour. The tempo of gait was not specified. The measured data consisted of angular data of both hip joints measured by potentiometers and internal pressure data of the PAM, to which an appropriate differential filter was applied to obtain angular velocity, angular acceleration, and pressure differential values. A low-pass filter (cutoff frequency was 5.0 Hz) was applied for the joint angle and a band-pass filter (passband width was 0.2 to 2.0 Hz) for the PAM internal pressure. The experiment was conducted on a treadmill capable of emergency stops, and the experimenter remained near the treadmill at all times during the experiment so that the subject could be immediately protected in the event of an emergency. This experiment was conducted with the approval of the Ethics Committee of the Graduate School of Information Science and Technology of the University of Tokyo (review number: UT-IST-RE-210702-1) and the participants signed consent forms. The same applies to the experiments described in Section IV.

The joint states to be estimated are the angles, angular velocities, and angular accelerations of the right and left hip joints in a total of six dimensions. The average of the squared error in each dimension divided by the variance is used as one of the estimation performance indicators. In other words, when X_i is the posture information in each dimension, the index obtained by

$$error = \frac{1}{6}\sum_i \frac{\text{MSE}\,(X_i)}{\text{Var}\,(X_i)} \tag{6}$$

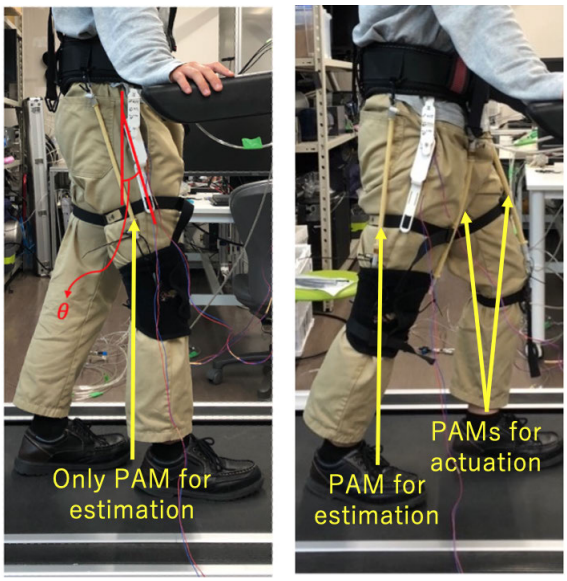

FIGURE 4. The conditions of the experiments (left: offline; right: online). θ is a measured joint angle.

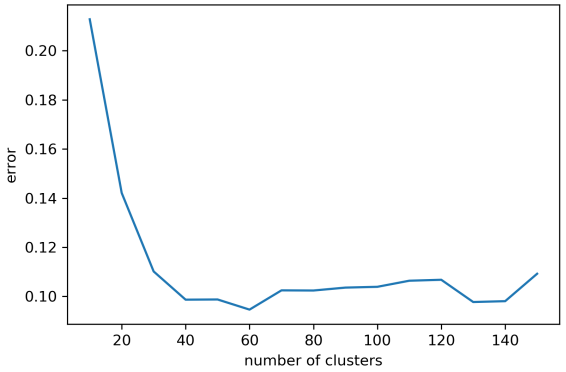

FIGURE 5. Optimization of the number of clusters.

is called the average error in all dimensions. The optimization of the number of clusters, which is a hyper parameter in this estimation method, was performed under four cross-validations based on the all-dimensional mean error index defined above. The results are shown in Fig. 5.

While the number of clusters is small, increasing the number of clusters improves the resolution and accuracy of estimation. On the other hand, as the number of clusters increases, the accuracy tends to deteriorate as the difference between clusters disappears and transitions are more likely to fail. When actually assisting, cross-validation should be performed in each case, and the appropriate number of clusters should be tuned.

Fig. 6 shows the estimation results for all six dimensions with the number of clusters set to 60. In the figure, the blue line shows the measured values and the orange line shows the estimated values, and LH and RH refer to the left and right hip joints, respectively. It can be seen that the multi-dimensional information of multiple joints can be estimated

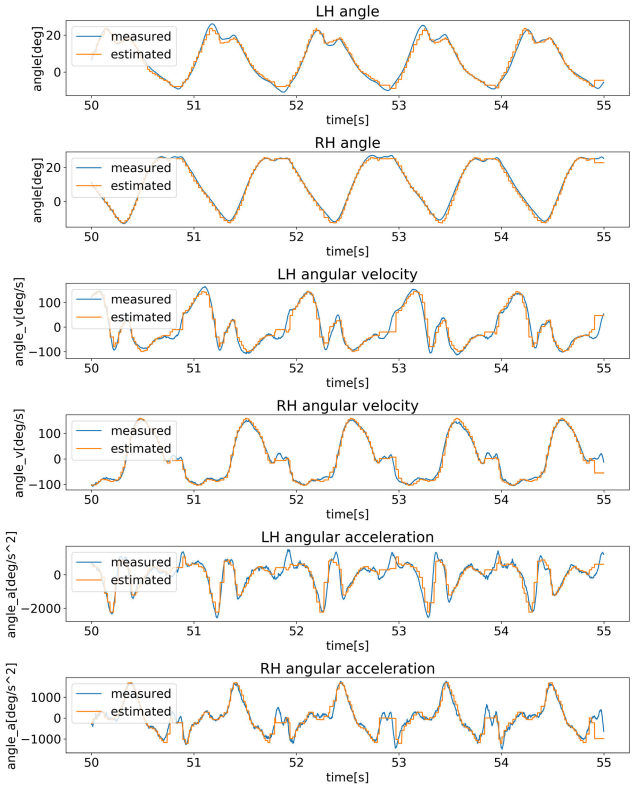

FIGURE 6. Offline estimation result.

from only a single PAM internal pressure information. Since the algorithm assigns clusters closest to the input data, it was expected that the estimated values would be stepped, but if the number of clusters is sufficiently large, it can be seen that the estimation is continuous. In the angular acceleration, the estimation error is instantaneously a little larger near the sharp extremes, but this is thought to be due to the flattening of the spike-like waveform to assign the average within a cluster. The reason why the estimation error is smaller for the right leg than for the left is thought to be because the artificial muscle for estimation is attached to the lateral part of the right thigh, and the mechanical movement of the right leg is more directly reflected in the internal pressure.

The average time required for joint state estimation was 5.24×10^{-6} s under Ubuntu 18.04.6 Intel Core-i9 with 8 physical cores, which is a small enough amount of computation to control the robot at a sampling rate of 500 Hz and we confirmed that real-time performance was achieved.

Since the clusters to be compared are limited by the immediately preceding cluster, the estimation method is very robust against instantaneous noise. Also, even if the estimation is wrong, it is guaranteed not to output estimates with extremely large errors, since the estimated values are the average posture states of neighboring walking phases. Therefore, the risk of dangerous assist control due to this is low, and it can be said to be a safe estimation method that is friendly to the wearer.

In this study, the proposed method was used only for estimating the state of both hip joints. In future research, it is assumed that estimation of multiple joints related to walking, such as the knee and ankle joints, will be performed, but we believe that scaling will be easily possible by expanding the number of dimensions of $\vec{S}_n$ described above. Moreover, although the input dimension is two-dimensional, consisting only of the internal pressure of a single PAM and its derivative in this method, it is easy to extend this dimension, too.

D. ROBUSTNESS VERIFICATION

The gait may gradually become unsteady due to fatigue or other factors caused by continuous use of the device. The proposed method is an interpolation algorithm that searches for the data closest to the current gait phase in the training data, so there is a possibility that the estimation accuracy will deteriorate if the gait is different from the gait at the time the training data was acquired. Therefore, in this section, we examine the robustness of the proposed posture estimation method against changes in gait.

Since it is dangerous and complicated to conduct experiments under conditions that create a sense of fatigue, in this study, we intentionally acquired data that imitated the gait that changed under one subject and verified the accuracy of the posture state estimation offline.

In this study, walking on a treadmill with a fixed speed is assumed, so the walking tempo and stride length are inversely proportional to each other. Therefore, the following two main cases are assumed to occur when the gait changes due to fatigue.

- The case in which fatigue causes the stride length to decrease and the gait tempo to increase.
- The case in which fatigue causes the gait tempo to decrease and the stride length to increase.

The specific experimental procedure was as follows.

1. Angle sensors and the assistive robot were attached to the walker.
2. Walking on a treadmill at a speed of 5 km/h without fixing the tempo, the angle data of both hip joints and the internal pressure data of the PAM for estimation were acquired for 30 seconds (the data at this time will be referred to as the data during Not fix).
3. From the data during Not fix, we calculated the average tempo by dividing the walking time by the number of cycles.
4. Fix the tempo to several values different from the tempo calculated above, walk on a treadmill at a speed of 5 km/h, and acquire data for 10 seconds each time.
5. The first 20 seconds of the data during Not fix was used as training data, and training was performed using the method described above.
6. Verify the estimation accuracy based on the remaining 10 seconds of the data during Not fix and the multi-tempo data obtained in item 4.

As for item 3 above, the data for 30 cycles were trimmed appropriately, and the interval was 28.94 seconds, so the average tempo was estimated to be 124.4 BPM. Therefore,

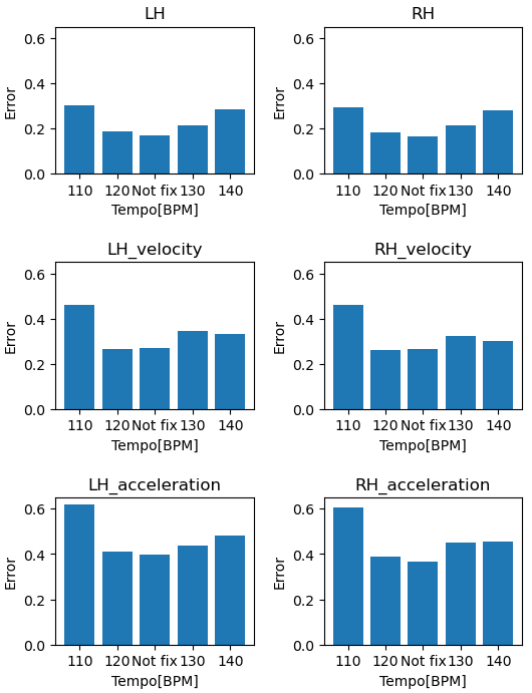

FIGURE 7. Estimation errors at different tempos.

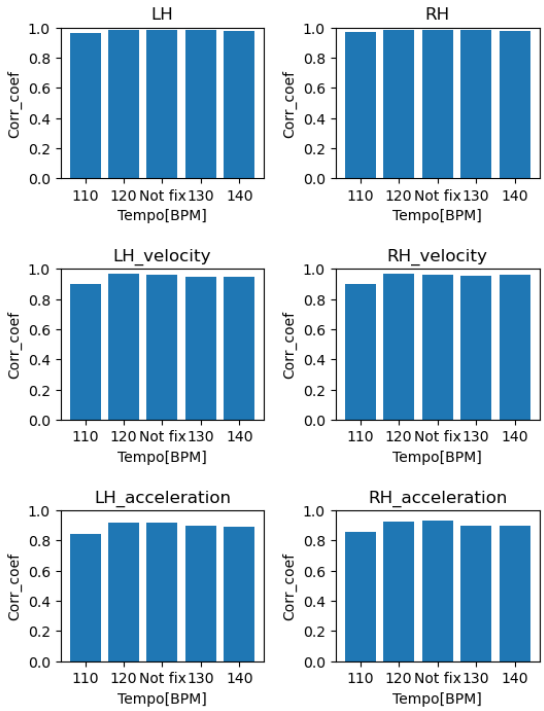

FIGURE 8. Correlation coefficients at different tempos.

measurements in item 4 were taken at 110, 120, 130, and 140 BPM to simulate a disordered gait. Walking at a tempo lower than 110 BPM and higher than 140 BPM was not measured because it was very unstable, and there were safety concerns. The walking tempo was fixed by having the walkers walk while listening to the metronome through earphones, and this method was also used in the experiments described in the following chapters. The number of clusters was determined to be 60 with appropriate cross-validation.

Fig. 7 is a bar chart for the error in each data set. In the figure, LH and RH refer to the left and right hip joints, respectively. The error indices were calculated by dividing the RMSE of each dimension by the standard deviation of the measured data. As a general trend, the further away from the average tempo at the time of the Not fix, i.e., 124.4 BPM, the greater the error. If the tempo deviation is 120 130 BPM, the error is only 1.3 times larger at most.

In addition, the essence of this estimation method is to ''continuously synchronize the human and robot motions'' rather than to ''estimate the joint state with the smallest possible error.'' Therefore, the correlation coefficient between the measured and estimated values was used as another evaluation index. The results are shown in Fig. 8. The fact that the correlation coefficient hardly changes even if the walking tempo changes compared to the not-fixed tempo suggests that even if the tempo differs from that at the time of training data acquisition, the estimation can be synchronized with the wearer's movements. This means that human and robot synchronization can be maintained.

One factor that guarantees robustness is the normalization process. To be precise, the internal pressure of the PAM for estimation is not used as is but is normalized before being used for estimation. That can contribute to the robustness to changes in gait. Note that the device can stop use to avoid serious accidents when there is an extreme change in gait.

III. PROPOSED CONTROL METHOD

A schematic diagram of the entire control method divided into modules is shown in Fig. 9. u is the input voltage to the valve, F and L are the contraction force and length of the PAM for actuation, respectively, and P_{ref} and P are the target internal pressure and measured pressure of the PAM for actuation, respectively.

θ, $\dot{\theta}$, and $\ddot{\theta}$ are the angle, the angular velocity, and the angular acceleration of both hip joints estimated by the algorithm described in Section II. The control calculation process consists of the following four steps.

1. Calculate the torque generated at the joint based on the estimated joint information.
2. Calculate the contraction force and length of the PAM geometrically.
3. Calculate the required internal target pressure P_{ref} based on Mckibben PAM model.
4. Control the valve by PI controller to perform pressure follow-up control.

A. CALCULATION OF THE TORQUES

As a dynamic model of the walking human, consider a 5-link system as shown in Fig. 10. The moment of inertia around the center of gravity at link i is defined as I_i, mass as m_i, and length as l_i. The distance from Joint 1 to the centers of gravity

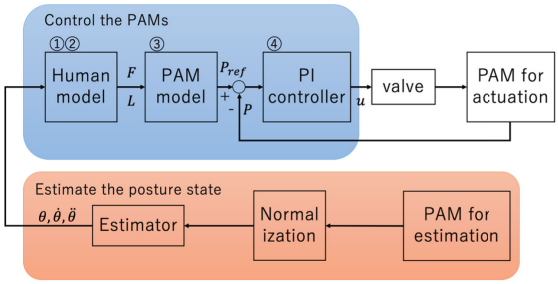

FIGURE 9. Proposed control method.

of Link 1 and Link 2 are a_1 and a_2, respectively, the distance from Joint 2 to the centers of gravity of Link 3 and Link 4 are a_3 and a_4, respectively, and the distance from Joint 3 to the center of gravity of Link 5 is a_5. Since the purpose of this study is to verify the effectiveness of the estimation algorithm by applying it to gait-assistive control for the first time, only hip flexion motion is considered as an assist target for simplicity. In this case, since the influence of knee and ankle angles changes during walking is sufficiently small, the entire leg is assumed to be a single link for calculating the hip joint torque. We also assumed that the upper body is always vertical to the ground, and the ankle joint is always at right angles for simplify the calculation as follows.

$$\begin{aligned} &\theta_2, \theta_3 \cong 90 \text{ deg (const)} \\ &\theta_5 \cong \theta_4 - 270 \text{ deg (const)} \end{aligned} \tag{7}$$

In this study, we determined the subject's body feature parameters appropriately based on measurements at each site and research by Ae et al. [39]. The determination of swing leg in applying the mechanical model is based on the hip joint angular velocity information. That is, when the left and right hip joint angular velocities are $\dot{\theta}_{LH}$ and $\dot{\theta}_{RH}$, respectively, the swing leg is determined as follows.

$$\begin{aligned} &\text{if } \dot{\theta}_{LH} > 0 \text{ and } \dot{\theta}_{RH} < 0\text{: Left} \\ &\text{else if } \dot{\theta}_{LH} < 0 \text{ and } \dot{\theta}_{RH} > 0\text{: Right} \\ &\text{else: Same as just before} \end{aligned}$$

Note that in this study, the time when both feet are landing is not considered. The equations of motion at each link can be solved analytically as follows.

$$\begin{aligned} v_1 &= M_1 f + g \\ v_2 &= M_2 \tau + M_3 f + v_3 \end{aligned} \tag{8}$$

v_1: Vector of mass × acceleration for each link
M_1: Appropriate constant matrix
f: Vectors of external forces between joints
g: Vector for the gravity term
v_2: Vector of moment of inertia × angular acceleration of each link
M_2: Appropriate constant matrix
τ: Torque vector generated at joints
M_3: Appropriate matrix
v_3: Vectors on friction terms, etc.

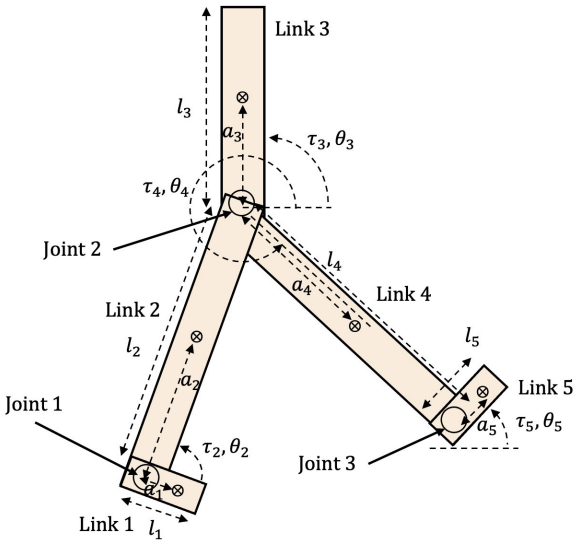

FIGURE 10. 5-link human model.

By substituting the estimated joint states into the above equations as appropriate, the vector τ, which lines up the torques produced at each joint, is obtained as follows, part of which is the assist torque. r is the assist rate.

$$\begin{aligned} \tau &= M_2^{-1}\left[v_2 - \left\{M_3 M_1^{-1}(v_1 - g) + v_3\right\}\right] \\ \tau_{PAM} &= r\tau \quad (0 < r < 1) \end{aligned} \tag{9}$$

B. CALCULATION OF CONTRACTION FORCE AND LENGTH OF PAM

The length and contraction force of the PAM are calculated from the fixation position determined by various parameters. The fixation positions of the PAM for actuation are shown in Fig. 11. The length L of the PAM is the distance between the coordinates of both end points $|\vec{A_1A_2}|$ minus the length L_{fix} of the clasp, belt, supporter, and metal part. L_{fix} should be obtained by measurement or other means.

$$L = |\vec{A_1A_2}| - L_{fix} \tag{10}$$

The contraction force of the PAM corresponding to the direction of the torque is obtained as follows.

$$F = \max\left(\tau_{PAM}/d_{arm}\ 0\right) \tag{11}$$

Note that d_{arm} represents the length of the moment arm corresponding to the artificial muscle, which is calculated by the distance between the point O and the line A_1A_2.

C. MCKIBBEN PAM MODEL

The contraction force $F(P, L)$ of a Mckibben PAM has been modeled by Tagami et al. [40]. in their study as a two-variable function of internal pressure and length. The various parameters are shown in Table 2.

$$F(P, L) = K_g(P - P_{th})(L - L_{min}) + K_{pr}(L - L_0) + nl(L) \tag{12}$$

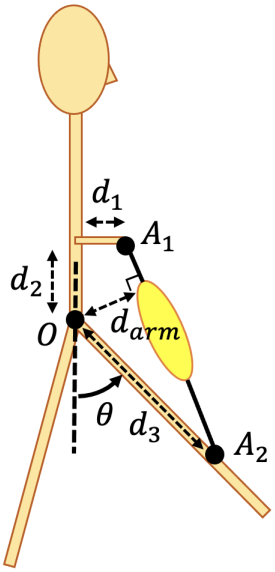

FIGURE 11. Position of the PAM for actuation.

TABLE 2. Mckibben PAM parameters.

Parameter	Value
K_g [N/(Pa · m)]	9.91×10^{-3}
K_{pr} [N/m]	3.69×10^{-3}
P_{th} [Pa]	4.47×10^{4}
L_{min} [m]	180×10^{-3}
L_0 [m]	250×10^{-3}
$nl(L)$ [N]	0

where P_{th} is the pressure that gives the threshold value and L_{min} and L_0 are the length of the PAM at its minimum and initial length, respectively. The internal pressure can be obtained from the contraction force and length, which is used as the target internal pressure P_{ref} of the PAM.

D. PI CONTROLLER

We control the internal pressure of the PAM by a simple PI controller. When P does not reach P_{ref}, the input voltage to the servo valve is increased and the effective area of the valve is adjusted to control the air flow rate to follow the internal pressure.

E. STOP DETECTION

For switching control of start and stop walking, the determination that a subject has stopped walking is based on a threshold value. Specifically, the internal pressure values of the PAM for estimation for the past T seconds are buffered, and when the maximum and minimum values in the buffer are p_{max} and p_{min}, respectively, and the following equation is satisfied under the appropriate threshold value p_{stop}, the target pressure value P_{ref} is set to 0 and the assistive suit is stopped. In this study, T was experimentally determined to be 5 s and p_{stop} was set as 0.15 kPa.

$$p_{max} - p_{min} < p_{stop} \tag{13}$$

TABLE 3. Control parameters.

Parameter	Value
K_p [V/kPa]	0.07
K_i [V/kPa×s]	0.00
Passband width of band-pass filter of PAM pressure for estimation [Hz]	0.2 to 2.0
Cut-off frequency of low-pass filter of hip angle [Hz]	5.0
Cut-off frequency of low-pass filter of PAM pressure for actuation [Hz]	10.0
Initial pressure of PAM for estimation [kPa]	Approximately 1.00×10^2
P_s [kPa]	Approximately 7.50×10^2
Number of clusters	60
n_{th}	50
α	1.00
r	0.20
Training data length [s]	10.0
l_1, l_5 [m]	0.25
l_2, l_4 [m]	0.79
l_3 [m]	0.87
m_1, m_5 [kg]	1.34
m_2, m_4 [kg]	10.78
m_3 [kg]	46.14
I_1, I_5 [kg · m^2]	1.90×10^{-3}
I_2, I_4 [kg · m^2]	0.48
I_3 [kg · m^2]	2.50
a_1, a_5 [m]	0.08
a_2, a_4 [m]	0.48
a_3 [m]	0.42
L_{fix} [m]	0.17
d_1 [m]	0.05
d_2 [m]	0.05
d_3 [m]	0.37
Coefficient of friction at joints [kg · m^2/s]	0.10

IV. RESULTS

A. CONTROL EXPERIMENT

We first conducted an experiment on a single subject to test the proper control of the gait-assistive robot. Walking was performed on an electric treadmill moving at 5[km] per hour. The tempo of walking was not specified. The experimental procedure consisted of the following three parts.

1. We acquired PAM internal pressure and bilateral hip joint condition data for estimation during normal walking for 90 seconds.
2. We trained with the acquired gait data.
3. We controlled the PAMs and walk for 90 seconds with gait assist.

The assist experiment is shown in the right side of Fig. 4. The PAM for estimation is attached to the lateral part of the right thigh, and the PAM for actuation is attached to the anterior part of both thighs.

The various parameters used in the experiment are shown in Table 3. The number of clusters was appropriately determined through cross-validation, and P_s is the supply side pressure by the regulator, which was manually adjusted.

Fig. 12 shows the results of online estimation of hip angle, angular velocity, and angular acceleration during assist. In the figure, the blue and orange lines indicate measured and estimated values, respectively, where LH and RH refer to the left and right hip joints, respectively. It can be seen that

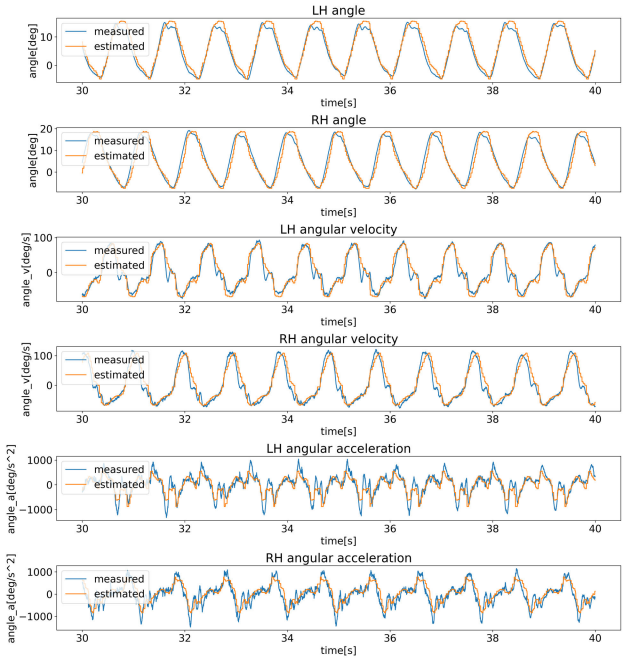

FIGURE 12. Results of the online posture estimation.

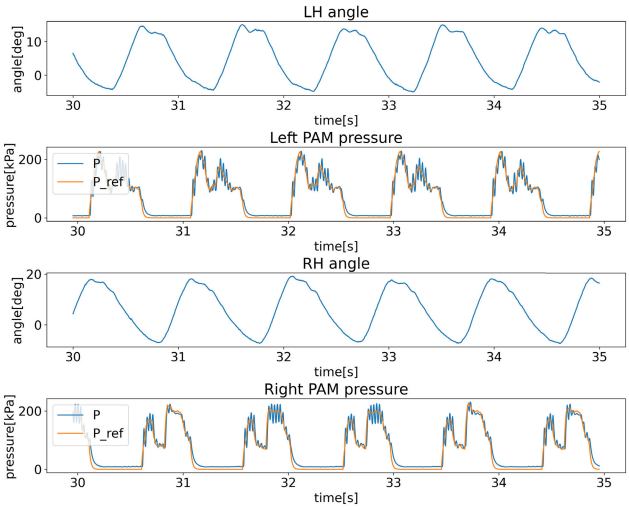

FIGURE 13. Follow-up control of the PAM pressure.

the change in gait due to assist is negligibly small, and the posture state can be estimated correctly as in the offline case in Section II-C. The RMSE of the hip joint angle estimation was 1.58 deg and 2.39 deg for the left and right hip joints, respectively.

An evaluation of the pressure tracking control performance of the left and right PAMs is shown in Fig. 13. Note that a low-pass filter with a cutoff frequency of 10 Hz is applied to the pressure waveforms. The first and third rows are the left and right hip joint angle transition, and the second and forth rows are results of pressure tracking control, with the blue and orange lines corresponding to the PAM internal pressure and target internal pressure, respectively. First, it can be seen that the PAM internal pressure is following the target pressure by PI control. Also, it can be seen that the target pressure waveform (P_{ref} in the figure) is generated smoothly by the state estimation of both hip joints. In addition, it can be seen that the PAM internal pressure increases and contracts during the time period when the hip joint angle begins to increase, assisting the swing up.

B. EMG EXPERIMENT

Next, we conducted an experiment to verify the assist performance with three subjects. Although it is possible to control the assist suit without fixing the gait tempo, for the sake of myoelectric analysis, the experiment was conducted with the gait tempo fixed. In addition, a manual treadmill was used to prevent noise from being mixed into the myoelectric data. The experimental procedure is as follows.

1 Practice the task of walking at 5 km per hour and 120 BPM for 30 seconds.
2 Attach the angle sensor and the gait-assistive robot.
3 Record the PAM internal pressure and hip joint condition during normal walking for 60 seconds as training data.
4 Take off the angle sensor and the gait-assistive robot.
5 5-minute break
6 Train with acquired gait data.
7 Attach surface EMG electrodes.
8 Measure EMG during MVC (Maximum Voluntary Contraction).
9 Walk without assistance for 90 seconds and measure the EMG.
10 Wear the gait-assistive robot.
11 Practice walking with assistance; check for 20 seconds and add 20 seconds at a time until familiar.
12 Perform walking with assist for 90 seconds and measure EMG.

The EMG measurement points were two on the subject's left leg: the adductor longus (AL) muscle, which is primarily involved in the hip flexion movement of the leg, and the semitendinosus (ST) muscle. The EMG of the ST, the antagonist muscle of the AL, was also measured to ensure that the assist force was not interfering with the subject's ability to perform the hip extension movement.

Table 4 lists the physical parameters of each subject and the number of clusters optimized for each individual. Various body information parameters such as moment of inertia, mass, and length of each body part were appropriately corrected based on height and weight ratios.

To evaluate the performance of the EMG amplitude, we used the %MVC index, which is expressed by the following equation.

$$\%MVC = 100 \times \frac{J}{J_{MVC}} \tag{14}$$

$$J = \sqrt{\frac{1}{T}\int_{T_{cycle\_start}}^{T_{cycle\_end}} EMG^2 dt} \tag{15}$$

TABLE 4. Subjects' parameters for control.

	Height [m]	Weight [kg]	L_{fix} [m]	Number of clusters
Subject 1	1.62	55	0.17	60
Subject 2	1.71	70	0.18	30
Subject 3	1.68	56	0.18	20

Here, the average EMG amplitude J was calculated for each gait cycle after applying the appropriate high-pass, low-pass, and bandstop filtering to the EMG data; for J_{MVC}, the EMG amplitude data were obtained during maximal contraction, of which the average amplitude for 1 s was calculated. The sensor position and clinical test method for measuring MVC status were determined based on the SENIAM project [41].

Shown in Fig. 14 is a graph of %MVC values for AL and ST for three subjects, where Without assist refers to normal walking and With assist refers to gait with assistance. The bold bar means the average value and thin bar means standard deviation. Using 30 cycles of data for each subject, significant differences in %MVC values were calculated by Welch's t-test. The symbols ** and * in Fig. 14 indicate statistical differences at the 1% and 10% significance level for one-tailed tests.

In Subjects 1 and 2, the EMG amplitudes of both the AL and ST were significantly lower during assisted walking than during normal walking ($p < 0.01$). The reason for the decrease in the ST, which is not the muscle to be assisted, is that the AL and ST are antagonistically driven in terms of muscle structure, and the decrease in the activity of the anterior muscle, the AL, is thought to have been accompanied by a decrease in the activity of the posterior ST. For subject 3, although the amount of AL muscle activity was significantly reduced ($p < 0.10$), the amount of ST muscle activity was significantly increased during the assist ($p < 0.01$).

Fig. 15 shows the EMG amplitude data of the AL of the left leg and the internal pressure of the attached PAM for actuation on the left thigh for Subject 1. From the figure, it can be seen that the internal pressure of the PAM increases during the time of increased muscle activity of the AL. That means the PAM was able to synchronize with the AL muscle.

Fig. 16 shows the averages of 30 cycles of myoelectric amplitude absolute values of Subject 1, to which a low-pass filter with a cutoff frequency of 20 Hz was applied. From the graph, it can be seen that the amplitude of EMG of With assist is lower than that of Without assist especially at the moment of trying to swing up the hip joint, i.e., before and after the Pre-swing phase.

Fig. 17 shows the kernel density $\hat{f}(p, \dot{p})$ of the internal pressure value of PAM for estimation p and its derivative $\dot{p}$ for each subject. Gaussian kernel was used for the kernel, and the bandwidth h was set appropriately. K is the kernel function and n is the number of data.

$$\hat{f}(p, \dot{p}) = \frac{1}{nh^2} \sum_{i=1}^{n} K\left(\frac{p - p_i}{h}, \frac{\dot{p} - \dot{p}_i}{h}\right) \tag{16}$$

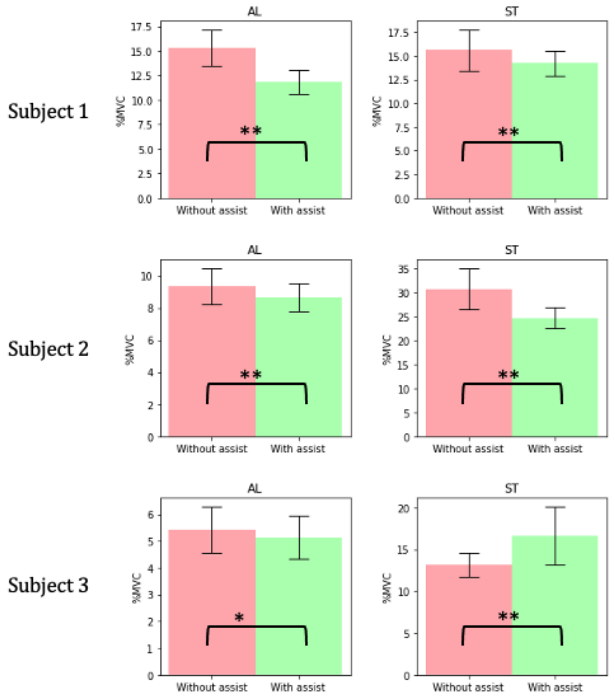

FIGURE 14. Results of the %MVC (mean and standard devation of 30 gait cycles).

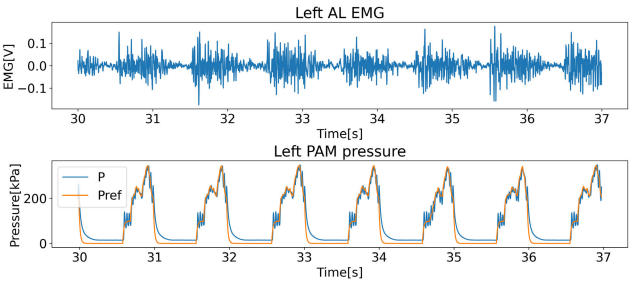

FIGURE 15. Change in EMG and internal pressure of PAM for actuation.

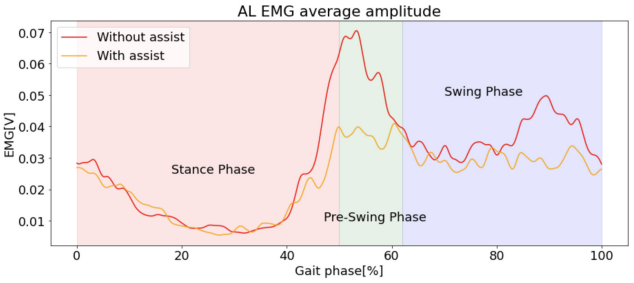

FIGURE 16. Average EMG amplitude within one gait cycle.

From Fig. 17, it can be seen that since walking is a cyclic motion, the density distribution of pressure and its derivative is cyclic for all subjects. Although there are some regions of concentration for each of the three subjects, especially for Subject 3's PAM, the density tends to be concentrated in a localized area. In other words, the pressure information in the PAM in Subject 3 did not change so much with the gait phase, and estimation was considered to be relatively difficult.

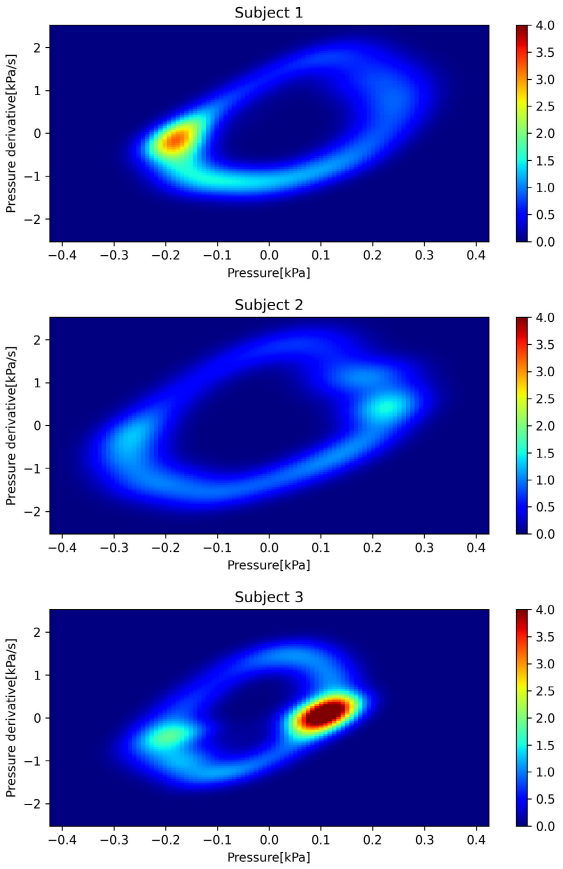

FIGURE 17. Density distribution of the internal PAM pressure and its derivative for each subject.

C. DISCUSSION

For the AL, the EMG amplitude was significantly reduced in all three subjects, suggesting the effectiveness of the assistive suit. Due to the fact that the AL and ST are antagonistically driven, assisting the AL simultaneously eliminates the force on the opposite side, which may be a secondary effect.

In addition, the fact that the contraction period of the PAM was the same as the activity period of the AL muscle, and the fact that the EMG amplitude decreased especially around the pre-swing phase, suggest that the ideal timing of control was achieved by using the postural state estimation method and the mechanical model of the walker.

Moreover, the results for subject 3 showed that the ST muscle was overloaded. There are two major possible reasons for this: one is that the PAM for driving the anterior thigh was fixed so tightly that external torque was generated on the hip flexor side even if the PAM did not contract. Another possibility is that an undesirable attachment of the suit adversely affected the estimation of the postural state, and that the suit control under this condition increased the difficulty of walking. From Fig. 17, for subject 3, the PAM internal pressure and its derivative values were locally concentrated throughout the gait cycle, which may have worsened the resolution of the postural state estimation and increased the estimation error.

The ideal solution would be to teach the preferred way of wearing, but it is extremely difficult to objectively observe the wearing condition and point it out by verbalization or other means. Another possible solution is to add PAMs for estimation, and even if the value of a single PAM stagnates, the estimation accuracy can be recovered by ensuring that other PAMs do not. However, this is contrary to the concept of the method of reducing the number of PAMs for estimation, and is also undesirable from the perspective of weight reduction. Overcoming this problem by devising an estimation algorithm is still an ongoing research issue.

V. CONCLUSION

The conclusions of this study are as follows.

First, we proposed a new algorithm to estimate the postural state of a wearer from a single PAM internal pressure information with a small computational complexity by utilizing a clustering method and the broad-sense periodicity of gait, and confirmed the estimation accuracy in offline experiments. Second, based on the estimated joint states of the lower limb and the assumed mechanical model of a human, we generated a continuous target internal pressure of the PAM for actuation and controlled the PAM under pressure-following control. Finally, we measured the AL muscle activity during normal and assisted walking for three subjects and performed a one-sided significance test using Welch's t-test, which yielded significant differences at the 1% significance level for two subjects and at the 10% significance level for the remaining subjects, allowing us to evaluate the effectiveness of the assistive robot.

In the present study, only the limited movement of hip flexion was targeted for the assist, but in future studies, the assist area may be expanded to include extension and ankle joint movement. It is also necessary to conduct research on subjective evaluation, such as how subjects feel when assisted. The postural state estimation method proposed in this paper could be applied to other movements with a broad sense of periodicity, such as swimming, running, and bicycling, in addition to walking.

ACKNOWLEDGMENT

The authors would like to thank Shingo Oono of Bridgestone Corporation for his support.

REFERENCES

[1] T. Yan, M. Cempini, C. M. Oddo, and N. Vitiello, "Review of assistive strategies in powered lower-limb orthoses and exoskeletons," *Robot. Auto. Syst.*, vol. 64, pp. 120–136, Feb. 2015, doi: 10.1016/j.robot.2014.09.032.

[2] K. H. Low, "Robot-assisted gait rehabilitation: From exoskeletons to gait systems," in *Proc. Defense Sci. Res. Conf. Expo (DSR)*, Aug. 2011, pp. 1–10, doi: 10.1109/DSR.2011.6026886.

[3] Z. Lovrenovic and M. Doumit, "Review and analysis of recent development of lower extremity exoskeletons for walking assist," in *Proc. IEEE EMBS Int. Student Conf. (ISC)*, May 2016, pp. 1–4, doi: 10.1109/EMBSISC.2016.7508620.

[4] Y. Sankai, "HAL: Hybrid assistive limb based on cybernics," in *Robotics Research*. Berlin, Germany: Springer, 2011, pp. 25–34, doi: 10.1007/978-3-642-14743-2_3.

[5] K. Yamamoto, M. Ishii, H. Noborisaka, and K. Hyodo, "Stand alone wearable power assisting suit–sensing and control systems," in *Proc. 13th IEEE Int. Workshop Robot Hum. Interact. Commun.*, Sep. 2004, pp. 661–666, doi: 10.1109/ROMAN.2004.1374841.

[6] T. Kanno, D. Morisaki, R. Miyazaki, G. Endo, and K. Kawashima, "A walking assistive device with intention detection using back-driven pneumatic artificial muscles," in *Proc. IEEE Int. Conf. Rehabil. Robot. (ICORR)*, Aug. 2015, pp. 565–570, doi: 10.1109/ICORR.2015.7281260.

[7] T. Miyazaki, T. Tagami, D. Morisaki, R. Miyazaki, T. Kawase, T. Kanno, and K. Kawashima, "A motion control of soft gait assistive suit by gait phase detection using pressure information," *Appl. Sci.*, vol. 9, no. 14, p. 2869, Jul. 2019, doi: 10.3390/app9142869.

[8] Y. Li and M. Hashimoto, "PVC gel soft actuator-based wearable assist wear for hip joint support during walking," *Smart Mater. Struct.*, vol. 26, no. 12, Oct. 2017, Art. no. 125003, doi: 10.1088/1361-665X/aa9315.

[9] Z. Lovrenovic and M. Doumit, "Development and testing of a passive walking assist exoskeleton," *Biocybern. Biomed. Eng.*, vol. 39, no. 4, pp. 992–1004, Oct. 2019, doi: 10.1016/j.bbe.2019.01.002.

[10] Y. Ikeuchi, J. Ashihara, Y. Hiki, H. Kudoh, and T. Noda, "Walking assist device with bodyweight support system," in *Proc. IEEE/RSJ Int. Conf. Intell. Robots Syst.*, Oct. 2009, pp. 4073–4079, doi: 10.1109/IROS.2009.5354543.

[11] Y. Yang, L. Ma, and D. Huang, "Development and repetitive learning control of lower limb exoskeleton driven by electrohydraulic actuators," *IEEE Trans. Ind. Electron.*, vol. 64, no. 5, pp. 4169–4178, May 2017, doi: 10.1109/TIE.2016.2622665.

[12] H. K. Kwa, J. H. Noorden, M. Missel, T. Craig, J. E. Pratt, and P. D. Neuhaus, "Development of the IHMC mobility assist exoskeleton," in *Proc. IEEE Int. Conf. Robot. Autom.*, May 2009, pp. 2556–2562, doi: 10.1109/ROBOT.2009.5152394.

[13] A. T. Asbeck, S. M. M. De Rossi, I. Galiana, Y. Ding, and C. J. Walsh, "Stronger, smarter, softer: Next-generation wearable robots," *IEEE Robot. Autom. Mag.*, vol. 21, no. 4, pp. 22–23, Dec. 2014, doi: 10.1109/MRA.2014.2360283.

[14] A. T. Asbeck, S. M. M. D. Rossi, K. G. Holt, and C. J. Walsh, "A biologically inspired soft exosuit for walking assistance," *Int. J. Robot. Res.*, vol. 34, no. 6, pp. 744–762, Mar. 2015, doi: 10.1177/0278364914562476.

[15] A. T. Asbeck, K. Schmidt, and C. J. Walsh, "Soft exosuit for hip assistance," *Robot. Auton. Syst.*, vol. 73, pp. 102–110, Nov. 2015, doi: 10.1016/j.robot.2014.09.025.

[16] Q. Liu, A. Liu, W. Meng, Q. Ai, and S. Q. Xie, "Hierarchical compliance control of a soft ankle rehabilitation robot actuated by pneumatic muscles," *Frontiers Neurorobot.*, vol. 11, p. 64, Dec. 2017, doi: 10.3389/fnbot.2017.00064.

[17] L. Cheng, M. Chen, and Z. Li, "Design and control of a wearable hand rehabilitation robot," *IEEE Access*, vol. 6, pp. 74039–74050, 2018, doi: 10.1109/ACCESS.2018.2884451.

[18] L. Tang, G. Liu, M. Yang, F. Li, F. Ye, and C. Li, "Joint design and torque feedback experiment of rehabilitation robot," *Adv. Mech. Eng.*, vol. 12, no. 5, May 2020, Art. no. 168781402092449, doi: 10.1177/1687814020924498.

[19] M. Yokota and M. Takaiwa, "Gait rehabilitation system using a non-wearing type pneumatic power assist device," *J. Robot. Mechatronics*, vol. 33, no. 4, pp. 927–934, Aug. 2021, doi: 10.20965/jrm.2021.p0927.

[20] S. Hu, K. Fjeld, E. V. Vasudevan, and K. J. Kuchenbecker, "A brake-based overground gait rehabilitation device for altering propulsion impulse symmetry," *Sensors*, vol. 21, no. 19, p. 6617, Oct. 2021, doi: 10.3390/s21196617.

[21] Y. Muramatsu and H. Kobayashi, "Assessment of local muscle fatigue by NIRS—Development and evaluation of muscle suit," *ROBOMECH J.*, vol. 1, no. 1, pp. 1–11, Nov. 2014, doi: 10.1186/s40648-014-0019-2.

[22] H.-G. Kim, J.-W. Lee, J. Jang, C. Han, and S. Park, "Mechanical design of an exoskeleton for load-carrying augmentation," in *Proc. IEEE ISR*, Oct. 2013, pp. 1–5, doi: 10.1109/ISR.2013.6695682.

[23] T. Wang, Y. Zhu, T. Zheng, D. Sui, S. Zhao, and J. Zhao, "PALExo: A parallel actuated lower limb exoskeleton for high-load carrying," *IEEE Access*, vol. 8, pp. 67250–67262, 2020, doi: 10.1109/ACCESS.2020.2986357.

[24] A. B. Zoss, H. Kazerooni, and A. Chu, "Biomechanical design of the Berkeley lower extremity exoskeleton (BLEEX)," *IEEE/ASME Trans. Mechatronics*, vol. 11, no. 2, pp. 128–138, Apr. 2006, doi: 10.1109/TMECH.2006.871087.

[25] M. Dzahir and S.-I. Yamamoto, "Recent trends in lower-limb robotic rehabilitation orthosis: Control scheme and strategy for pneumatic muscle actuated gait trainers," *Robotics*, vol. 3, no. 2, pp. 120–148, Apr. 2014, doi: 10.3390/robotics3020120.

[26] K. Kadota, M. Akai, K. Kawashima, and T. Kagawa, "Development of power-assist robot arm using pneumatic rubbermuscles with a balloon sensor," in *Proc. 18th IEEE Int. Symp. Robot Hum. Interact. Commun. (RO-MAN)*, Sep. 2009, pp. 546–551, doi: 10.1109/ROMAN.2009.5326335.

[27] K. Tadano, M. Akai, K. Kadota, and K. Kawashima, "Development of grip amplified glove using bi-articular mechanism with pneumatic artificial rubber muscle," in *Proc. IEEE Int. Conf. Robot. Autom.*, May 2010, pp. 2363–2368, doi: 10.1109/ROBOT.2010.5509393.

[28] S. Sridar, Z. Qiao, N. Muthukrishnan, W. Zhang, and P. Polygerinos, "A soft-inflatable exosuit for knee rehabilitation: Assisting swing phase during walking," *Frontiers Robot. AI*, vol. 5, p. 44, May 2018, doi: 10.3389/frobt.2018.00044.

[29] D.-H. Lim, W.-S. Kim, H.-J. Kim, and C.-S. Han, "Development of real-time gait phase detection system for a lower extremity exoskeleton robot," *Int. J. Precis. Eng. Manuf.*, vol. 18, pp. 681–687, May 2017, doi: 10.1007/s12541-017-0081-9.

[30] Z. Ding, C. Yang, K. Xing, X. Ma, K. Yang, H. Guo, C. Yi, and F. Jiang, "The real time gait phase detection based on long short-term memory," in *Proc. IEEE 3rd Int. Conf. Data Sci. Cyberspace (DSC)*, Jun. 2018, pp. 33–38, doi: 10.1109/DSC.2018.00014.

[31] F. Wang, L. Yan, and J. Xiao, "Human gait recognition system based on support vector machine algorithm and using wearable sensors," *Sensors Mater.*, vol. 31, no. 4, pp. 1335–1349, Apr. 2019, doi: 10.18494/SAM.2019.2288.

[32] S.-S. Lee, S. T. Choi, and S.-I. Choi, "Classification of gait type based on deep learning using various sensors with smart insole," *Sensors*, vol. 19, no. 8, p. 1757, Apr. 2019, doi: 10.3390/s19081757.

[33] D. J. Villarreal, H. A. Poonawala, and R. D. Gregg, "A robust parameterization of human gait patterns across phase-shifting perturbations," *IEEE Trans. Neural Syst. Rehabil. Eng.*, vol. 25, no. 3, pp. 265–278, Mar. 2017, doi: 10.1109/TNSRE.2016.2569019.

[34] D. Quintero, D. J. Lambert, D. J. Villarreal, and R. D. Gregg, "Real-time continuous gait phase and speed estimation from a single sensor," in *Proc. IEEE Conf. Control Technol. Appl. (CCTA)*, Aug. 2017, pp. 847–852, doi: 10.1109/CCTA.2017.8062565.

[35] J. Perry and J. M. Burnfield, *Gait Analysis: Normal and Pathological Function*. Thorofare, NJ, USA: SLACK, 2010.

[36] T. Kawase, T. Miyazaki, T. Kanno, K. Tadano, Y. Nakajima, and K. Kawashima, "Pneumatic reservoir computing for sensing soft body: Computational ability of air in tube and its application to posture estimation of soft exoskeleton," *Sensors Mater.*, vol. 33, no. 8, pp. 2803–2824, Aug. 2021, doi: 10.18494/SAM.2021.3345.

[37] H. Hayashi, T. Kawase, T. Miyazaki, M. Sogabe, Y. Nakajima, and K. Kawashima, "Online assistance control of a pneumatic gait assistive suit using physical reservoir computing exploiting air dynamics," in *Proc. Int. Conf. Robot. Autom. (ICRA)*, May 2022, pp. 3245–3251, doi: 10.1109/ICRA46639.2022.9812377.

[38] J. MacQueen, "Some methods for classification and analysis of multivariate observations," in *Proc. 5th Berkeley Symp. Math. Statist. Probab.*, Jan. 1967, pp. 281–297.

[39] M. Ae, H.-P. Tang, and T. Yokoi, "Estimation of inertia properties of the body segments in Japanese athletes," (in Japanese), *Biomechanisms*, vol. 11, pp. 23–33, 1992, doi: 10.3951/biomechanisms.11.23.

[40] T. Tagami, T. Miyazaki, T. Kawase, T. Kanno, and K. Kawashima, "Pressure control of a pneumatic artificial muscle including pneumatic circuit model," *IEEE Access*, vol. 8, pp. 60526–60538, 2020, doi: 10.1109/ACCESS.2020.2983602.

[41] *The SENIAM Project*. Accessed: Apr. 5, 2023. [Online]. Available: http://www.seniam.org/

TETTA KADOKURA received the B.S. degree from the Department of Mathematical Engineering and Information Physics, The University of Tokyo, Tokyo, Japan, in 2021, where he is currently pursuing the master's degree in information physics. His research interests include power-assistive devices and control engineering.

TETSURO MIYAZAKI (Member, IEEE) received the Ph.D. degree in engineering from the Department of Mechanical Sciences and Engineering, Tokyo Institute of Technology, Tokyo, Japan, in 2014.

From 2014 to 2017, he was a Research Assistant (from 2014 to 2015) and an Assistant Professor (from 2015 to 2017) with Yokohama National University. From 2017 to 2020, he was an Assistant Professor with Tokyo Medical and Dental University. Since April 2020, he has been an Assistant Professor (from 2020 to 2021) and a Lecturer (since January 2022) with the Graduate School of Information Science and Technology, The University of Tokyo. His research interests include mechanical engineering, control engineering, power assistive devices, and medical welfare robotics.

TOSHIHIRO KAWASE (Member, IEEE) received the B.S., M.S., and Ph.D. degrees from the Tokyo Institute of Technology, Tokyo, Japan, in 2007, 2009, and 2012, respectively.

He was a Research Fellow with the Research Institute of National Rehabilitation Center for Persons with Disabilities, from 2012 to 2015, and a Postdoctoral Fellow and a specially appointed Assistant Professor with the Tokyo Institute of Technology, from 2015 to 2017. From 2017 to 2022, he was an Assistant Professor with Tokyo Medical and Dental University and the Tokyo Institute of Technology. Since April 2022, he has been an Associate Professor with Tokyo Denki University. His research interests include medical robots, rehabilitation robotics, and biological signal processing.

MAINA SOGABE received the veterinary and Ph.D. degrees in medicine from the Department of Medicine, Kyoto University, Kyoto, Japan, in 2015 and 2020, respectively.

From 2018 to 2020, she was a Researcher in intravital imaging and microscopic data processing with Kyoto University. Since October 2020, she has been a Researcher (from 2020 to 2022) and an Assistant Professor (since April 2022) with the Graduate School of Information Science and Technology, The University of Tokyo. Her research interest includes biomedical data processing and analysis.

KENJI KAWASHIMA (Member, IEEE) received the Ph.D. degree in engineering from the Department of Control Engineering, Tokyo Institute of Technology, Tokyo, Japan, in 1997.

From 1997 to 2000, he was a Research Assistant with the Tokyo Metropolitan College of Industrial Technology. He was an Associate Professor with the Precision and Intelligence Laboratory, Tokyo Institute of Technology. From 2013 to 2020, he was a Professor with Tokyo Medical and Dental University. Since April 2020, he has been a Professor with The University of Tokyo. His research interests include medical robotics, control engineering, and fluid measurement and control.